Turkish Journal of Earth Sciences

Manuscript 1921

Geomagnetic response to the earthquake in Türkiye and Syria on February 6, 2023

SVETLANA RIABOVA

SERGEY SHALIMOV

TÜBİTAK

Turkish Journal of Earth Sciences

http://journals.tubitak.gov.tr/earth/

Research Article

Turkish J Earth Sci
(2024) 33: 430-440

doi:10.55730/1300-0985.1921

Geomagnetic response to the earthquake in Türkiye and Syria on February 6, 2023

Svetlana RIABOVA[1,2,*], **Sergey SHALIMOV**[2]

[1]Sadovsky Institute of Geosphere Dynamics of Russian Academy of Sciences, Moscow, Russia
[2]Schmidt Institute of Physics of the Earth of the Russian Academy of Sciences, Moscow, Russia

Received: 16.11.2023 • **Accepted/Published Online:** 30.01.2024 • **Final Version:** 27.05.2024

Abstract: The disturbances in the lower ionosphere during the strong earthquake in Türkiye and Syria and its strongest aftershock on February 6, 2023, are analyzed using data from ground-based magnetometers. The observation points are located at distances 700 to 1600 km from the epicenter of the seismic event. As a characteristic of the ionospheric response to these events, variations in the magnetic field have been analyzed at the İznik, Grocka, Panagjurishte, and Surlari magnetic observatories. Earthquake epicenter is known to be a source of both seismic Rayleigh waves and atmospheric acoustic-gravity waves. Using the difference in velocities, at which these waves propagate from the epicenter, and their spectral composition, we found the ionospheric responses to the events that are interpreted quite well in terms of acoustic waves (produced by seismic Rayleigh wave) and atmospheric internal gravity waves generated in the earthquake epicenter.

Key words: Geomagnetic field, earthquake, seismic Rayleigh waves, atmospheric acoustic-gravity waves

1. Introduction

Studies of the impact of high-energy terrestrial sources, such as earthquakes, volcanoes, typhoons, and tsunamis on the human environment, as well as external geospheres are necessary to determine the mechanisms of these impacts in order to minimize the negative consequences of such influences. In the external geospheres, both atmosphere and ionosphere, the response to such events is currently being studied through various satellite systems. Thus, by measuring variations in the total electron content (TEC) (see, for example, (Dautermann et al., 2009; Kunitsyn et al., 2011), the ionospheric response to high-energy lithospheric sources is determined. Meanwhile, the traditional vertical sounding of the ionosphere by means of ground-based ionosondes also remains a fairly informative research tool. For example, (Maruyama et al., 2012) studied the response of the ionosphere after 43 earthquakes with magnitude ≥8 using ionograms from vertical sounding stations and found unusual ionograms (apparently due to the arrival of seismic Rayleigh waves) for 8 events out of 43. In this case, the stations with anomalous ionograms were located up to distances of 6000 km from the epicenter. It should be noted that as the distance from the epicenter increases, the probability of the intervention of external factors, which can also cause anomalous signals, increases. One of the main such factors is geomagnetic disturbances, against which one usually tries to find ionospheric responses to seismic events. Therefore, it is necessary to provide a special study in order to separate the contributions of various sources. This remark concerns not only the upper but also the lower ionosphere, variations which are often studied using magnetometers (Hao et al., 2013; Chernogor, 2019; Spivak and Riabova, 2019; Riabova and Shalimov, 2022).

In our work, using ground-based magnetometers, we analyze and interpret specific geomagnetic variations during the strong catastrophic earthquakes in Türkiye and Syria on February 6, 2023. Particular attention is paid to the influence of geomagnetic disturbances on the origin of signals.

The main shock of the earthquake with a magnitude of 7.8 (±0.1) was registered on February 6, 2023 at 4:17 LT (1:17 UT)[1]. The hypocenter was located in the Şehitkamil district of Gaziantep in Türkiye (Figure 1) near the border with Syria at a depth of 17.9 km. Geographical coordinates of the epicentre are: 37.174° N 37.032° E. Several thousand aftershocks were recorded after the earthquakes, with the magnitude of the strongest up to 7.5. The tremors, followed by several thousand aftershocks, were felt in eleven provinces of Türkiye and neighboring countries, mainly in

[1]USGS (2023). U.S. Geological Survey [Online]. Website https://earthquake.usgs.gov/ [accessed 2023/11/15].

* Correspondence: riabovasa@mail.ru

Syria. The strongest aftershock occurred at 10:24 UT (9 h after the main shock of the earthquake) and occurred in the Turkish region of Elbistan at a depth of 13.1 km. The geographical coordinates of the epicentre are 38.008° N 37.211° E.

It should be noted here that 11 min (1:28 UT) after the main shock, a rather powerful aftershock with a magnitude of 6.7 and a hypocentre depth of 14.5 km was registered. The epicenter coordinates are 37.127° N and 36.943° E. On the other hand, two more seismic events with a magnitude of 6.0 were registered (at the depth of 10 and 8.5 km with epicentre coordinates 37.127° N 36.943° E and 38.058° N 36.511° E, respectively) after the strongest aftershock. The first event occurred 2 min after the strongest aftershock (10:26 UT) and the second - at 12:02 UT.

The earthquake in Türkiye and Syria on February 6, 2023, is recognized as the most powerful in Türkiye since the 1939 earthquake in Erzincan. Türkiye is located in one of the most active seismic zones in the world. The area where the earthquake occurred is located at the intersection of three tectonic plates: Anatolian, Arabian, and African.

2. Initial data

We used the data of the geomagnetic field components recorded by ground-based magnetometers closest to the epicenters of the earthquake in Türkiye and Syria and strongest aftershock: İznik geomagnetic observatory (40.5° N 29.72° E; Türkiye); Surlari National Geomagnetic Observatory of the Geological Survey of Romania (44.68° N 26.25° E; Romania); Panagjurishte Geomagnetic Observatory (42.5° N 24.2° E; Bulgaria) and Grocka Geomagnetic Observatory of Republic Geodetic Institute (44.6° N 20.8° E; Republic of Serbia) (Figure 1). The distances from magnetic measurement points to the epicenter of the earthquake in Türkiye and Syria were: 1230 km (Surlari observatory), 1244 km (Panagjurishte observatory), and 1591 km (Grocka observatory). The distances from magnetic measurement points to the epicenter of the strongest aftershock in Türkiye and Syria were: 700 km (İznik observatory), 1175 km (Surlari observatory), 1211 km (Panagjurishte observatory) and 1553 km (Grocka observatory). Note that the distances are calculated using the haversine formula (van Brummelen, 2013).

We used magnetomer data with a sampling of 1 min, presented on the website of the INTERMAGNET International Network[2].

To characterize the geomagnetic situation during the main shock of the earthquake in Türkiye and Syria, we have chosen the following geomagnetic indices: Kpa, Kpm, Kp, ap and Dst, the values of which are presented by the International Service of Geomagnetic Indices[3]. In addition, we used information on minute variations in solar wind parameters (wind speed, B_z-component of the interplanetary magnetic field) obtained using the ACE satellite[4] and information about coronal holes on the Sun from the website of the Solar Dynamics Observatory[5]. It should be noted that prior to cross-wavelet analysis, the solar wind magnetic field data have been time shifted to the Earth's bow shock nose by assuming continuously varying planar solar wind phase fronts convecting with the solar wind (Weimer and King, 2008; Jackel et al., 2012).

3. Methods

When searching for a possible response of the geomagnetic field to a seismic event and analyzing its frequency composition, we used spectral analysis based on wavelets. Wavelet analysis provides noticeable advantages over classical spectral analysis and allows one to obtain temporal localizations of the spectral components of the time series (Foufoula Georgiou and Kumar, 1995; Torrence and Compo, 1998). Wavelet analysis makes it possible to reveal the temporal properties of the time series under study, to obtain local high-frequency and global large-scale information quite accurately and without redundancy, and also makes it possible to judge at what point in time certain signal components appeared (Percival and Walden, 2000). The method has proven itself well in the analysis of various nonstationary signals (Adhikari et al., 2017; Falayi et al., 2020; Zhao and Luo, 2021; Riabova, 2022). In our work, a continuous wavelet transform was used. In accordance with the theory of continuous wavelet transform (Daubechies, 1992), the coefficients of the time series $x(t)$ were defined as:

$$W(s,\tau) = \frac{1}{\sqrt{a}} \int_{-\infty}^{+\infty} x(t)\psi * \left(\frac{t-\tau}{s}\right) dt \,,$$

where s is the scale parameter, τ is the time shift parameter, $\psi\left(\frac{t-\tau}{s}\right)$ is the wavelet function obtained from the basis wavelet $\psi(t)$ by scaling and shifting in time, and the symbol * means complex conjugation. The wavelet projection consists in convolving the signal with an appropriate "focus kernel" ψ, which can be tuned with the scale parameter s in order to zoom in and out the details surrounding each point τ under analysis. By varying s and

[2]INTERMAGNET (2023). International Real-time Magnetic Observatory Network [Online]. Website https://www.intermagnet.org [accessed 2023/11/15].

[3]ISGI (2023). International Service of Geomagnetic Indices [Online]. Website http://www.isgi.unistra.fr [accessed 2023/11/15].

[4]NOAA (2023). ACE real-tıme solar wınd [Online]. Website https://www.swpc.noaa.gov/products/ace-real-time-solar-wind [accessed 2023/11/15].

[5]SDO (2023). Solar Dynamics Observatory [Online]. Website https://sdo.gsfc.nasa.gov/ [accessed 2023/11/15].

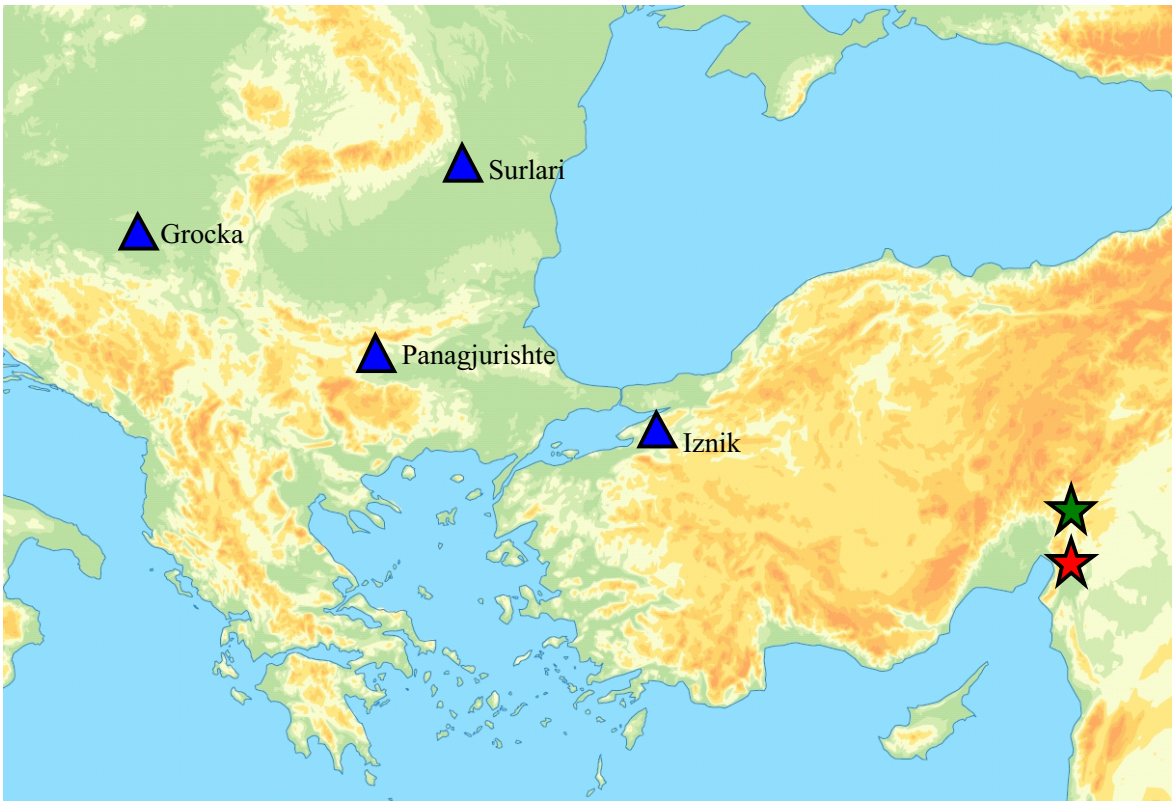

Figure 1. Layout of magnetometric stations (blue triangles). The epicenters of the earthquake and its strongest aftershock are marked with red and green asterisks.

τ, we can construct a picture showing both the amplitude of any features versus the scale and how this amplitude varies with time.

In our work, the Morlet wavelet, which is a plane wave modulated by a Gaussian of unit width, was used as the basic wavelet (Grossmann and Morlet, 1984):

$$\psi_0(t) = \pi^{1/4} \exp(0.5t^2)\left(\exp(i\omega_0 t) - \exp(-0.5\omega_0^2)\right),$$

where the second component in brackets can be neglected for .$\omega_0 = 2\pi > 0$

The visualization of the results of the wavelet transform during the present research was carried out by constructing the quantity $|W(s,\tau)|^2$, called the local energy spectrum or scalogram.

Due to the incomplete localization of the wavelet in time, "edge" effects may occur in the method of continuous wavelet transform (Meyer, 1993; Torrence and Compo, 1998). Therefore, in the present work, when performing the wavelet analysis, we built a cone of influence in which the "edge" effects cannot be ignored. The algorithm used in our work to perform wavelet analysis is described in detail in (Riabova, 2018).

In order to perform a comparative analysis of the variations in the B_z-component of the interplanetary magnetic field and the magnetic field components recorded at ground stations, the wavelet coherence of these time series was estimated (Grinsted, et al., 2004):

$$WC = \frac{|S(W_{IMF,B})|}{\sqrt{|S(W_{IMF})|}\sqrt{|S(W_B)|}},$$

where $W_{IMF,B}$ is a cross-wavelet spectrum, W_{IMF} is the wavelet spectrum of the variations B_z-component of the interplanetary magnetic field, W_B is a cross-wavelet spectrum of variations of the magnetic field components (total vector, horizontal and vertical components, northern and eastern horizontal components), the symbol S denotes preliminary smoothing of the signal before applying the wavelet transform to it in order to improve the time-frequency resolution and statistical significance (Maraun and Kurths, 2004). Wavelet coherence can take values from 0 to 1 and describes local correlations between two signals; the closer this value is to 1, the more correlated the signals are.

4. Geomagnetic situation during the earthquake

In order to detect geomagnetic anomalies accompanying a seismic event, in the present work an analysis of the geomagnetic situation was carried out. As parameters of geomagnetic activity, we considered temporal variations

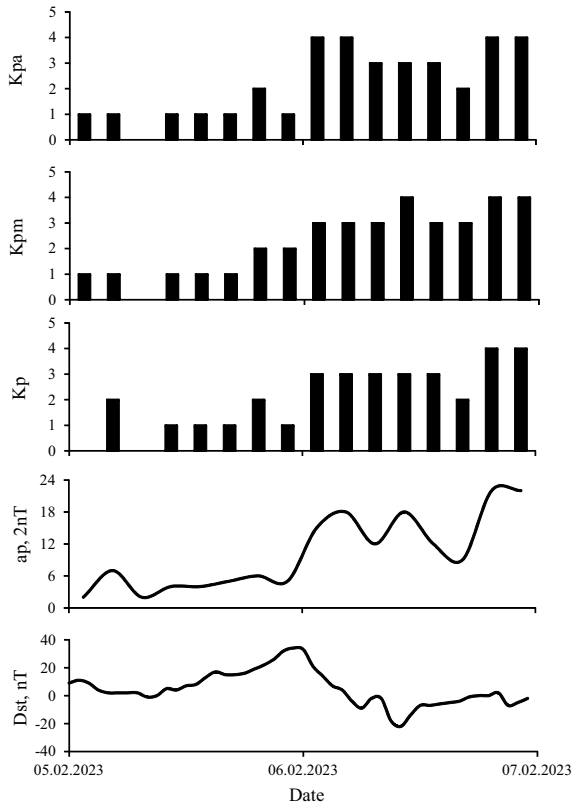

Figure 2. Temporal variations of geomagnetic indices: Kpa, Kpm, Kp, ap, and Dst from February 5 to February 6, 2023.

of the following geomagnetic indices: Kpa, Kpm, Kp, ap, and Dst. Time variations of all considered parameters of magnetic activity are shown in Figure 2. The data shown in Figure 2 indicate that in the period close to the main shock of the earthquake (1:17 UT) a moderate magnetic disturbance was observed, while the values of the three-h indices were Kpa = 4_+, Kpm = 3_+, Kp = 3_0, ap = 30 nT. In the course of Dst variations, a decrease was observed, which began at 0:00 UT from a value of 33 nT and ended at 10:30 UT, reaching a value of −22 nT.

In addition to the analysis of the parameters of magnetic activity, variations in the solar wind velocity and the B_z-component of the interplanetary magnetic field have been studied. Variations of these parameters are shown in Figure 3. The analysis of the data showed that, approximately from 22 UT on February 5, the fluctuations of the southern component increased to B_z = −11 nT and the solar wind speed began to increase, which was caused by the arrival of an inhomogeneous accelerated flow from a coronal hole of negative polarity that crossed the meridian on February 3–4. The maximum solar wind speed was reached at approximately 16 UT on February 6 and amounted to 420 km/s. We emphasize that at about 16 UT on February 6, another inhomogeneous accelerated stream from a coronal hole of negative polarity reached the Earth, which crossed the meridian on February 4–5. Since that time, a new increase in the solar wind speed began, which reached a maximum of 600 km/s at about 5 UT on February 7, at which time the southern component of the interplanetary magnetic field fluctuated from B_z = −10 nT to B_z = 7 nT.

It can be expected that such processes will cause a response in the magnetic field components recorded at ground stations (well known for stations at low latitudes; see, for example, (Kelley, 1989)). To test this assumption in the next section we present the results of a comparative analysis of the variations in the B_z-component of the interplanetary magnetic field (IMF) and the magnetic field components recorded at the Grocka, Panagjurishte, Surlari, and İznik ground stations.

5. Comparative analysis of variations in the B_z-component of the interplanetary magnetic field and components of the geomagnetic field recorded at ground stations

When performing a comparative analysis of variations in geomagnetic field on the Earth's surface and the B_z-component of the IMF, data from instrumental observations

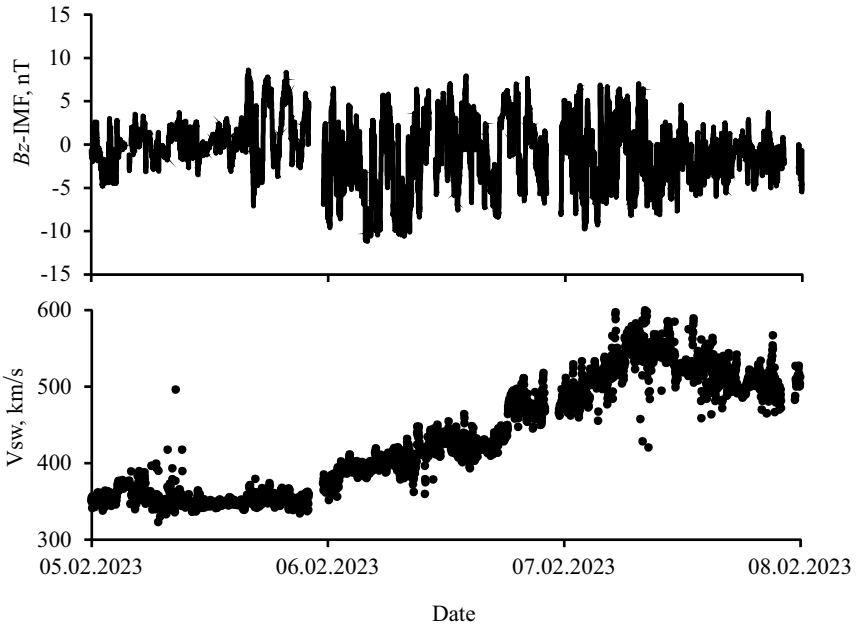

Figure 3. Variations of the B_z-component of the interplanetary magnetic field (B_z-IMF) and the solar wind velocity *V*sw from February 5 to February 7, 2023.

of geomagnetic variations recorded at the Grocka, Panagjurishte, Surlari, and İznik observatories were used.

First of all, we need to choose the component least affected by solar activity. For this purpose, a visual analysis of variations in the geomagnetic field components (total vector, horizontal and vertical components, northern and eastern horizontal components) was carried out.

Visual inspection showed, that with a delay of the first tens of min, geomagnetic field fluctuations repeat the general outlines of variations in B_z-component of the IMF. However, by visual examination of the data, we cannot judge the possible relationship between the variations in the geomagnetic field components and the change in the B_z-component of the IMF. Therefore, a cross-wavelet analysis was performed and five components of the magnetic field were considered.

During the cross-analysis of geomagnetic variations and the B_z-component of the IMF for about an h before the main shock of the earthquake and 5 h after it, similar results were obtained for all the observatories Grocka, Panagjurishte, and Surlari, so that we will present the results only for the Surlari observatory closest to the epicenter of the earthquake. It should be noted that during this period, the magnetic field was not registered at the İznik observatory.

The calculated coherences based on the wavelet transform of variations in the B_z-component of the IMF and five components of the geomagnetic field according to the Surlari observatory data are shown in Figure 4. The calculation was performed for a period of 6 h from the beginning of the day on February 6, 2023. Analysis of the data presented in Figure 4 showed that there are periods of high coherence for all components of the geomagnetic field. Also, it can be seen that a high coherence of the B_z-component of the IMF and four components (total vector, horizontal and vertical components, northern horizontal components) was observed. We note that from 1 UT to 4 UT in all components, except for the eastern horizontal component of the magnetic field, a high coherence is observed in the range of periods of 2–20 min, while the coherence in general is rather variable. The behavior of the eastern horizontal component of the magnetic field demonstrates a lower degree of coherence with variations in the B_z-component of the IMF. We note that during the main shock of the earthquake, and for almost 5 h after it the coherence not exceeded the value of 0.4. This means that the eastern horizontal component of the geomagnetic field is less sensitive to external source variations.

In the course of visual-comparative analysis and evaluation of wavelet coherence, we found that in the period one h before the aftershock with a magnitude of 7.5 and 5 h after it, the records of geomagnetic variations at the Grocka, Panagjurishte, Surlari, and İznik observatories were distorted by magnetic field variations caused by sources of solar origin, with the exception of the eastern horizontal component of the magnetic field.

Therefore, using the results of a comparative analysis of the variations in the geomagnetic field components recorded at the Grocka, Panagjurishte, Surlari, and İznik observatories, and the B_z-component of the IMF accompanying the main shock of the earthquake in

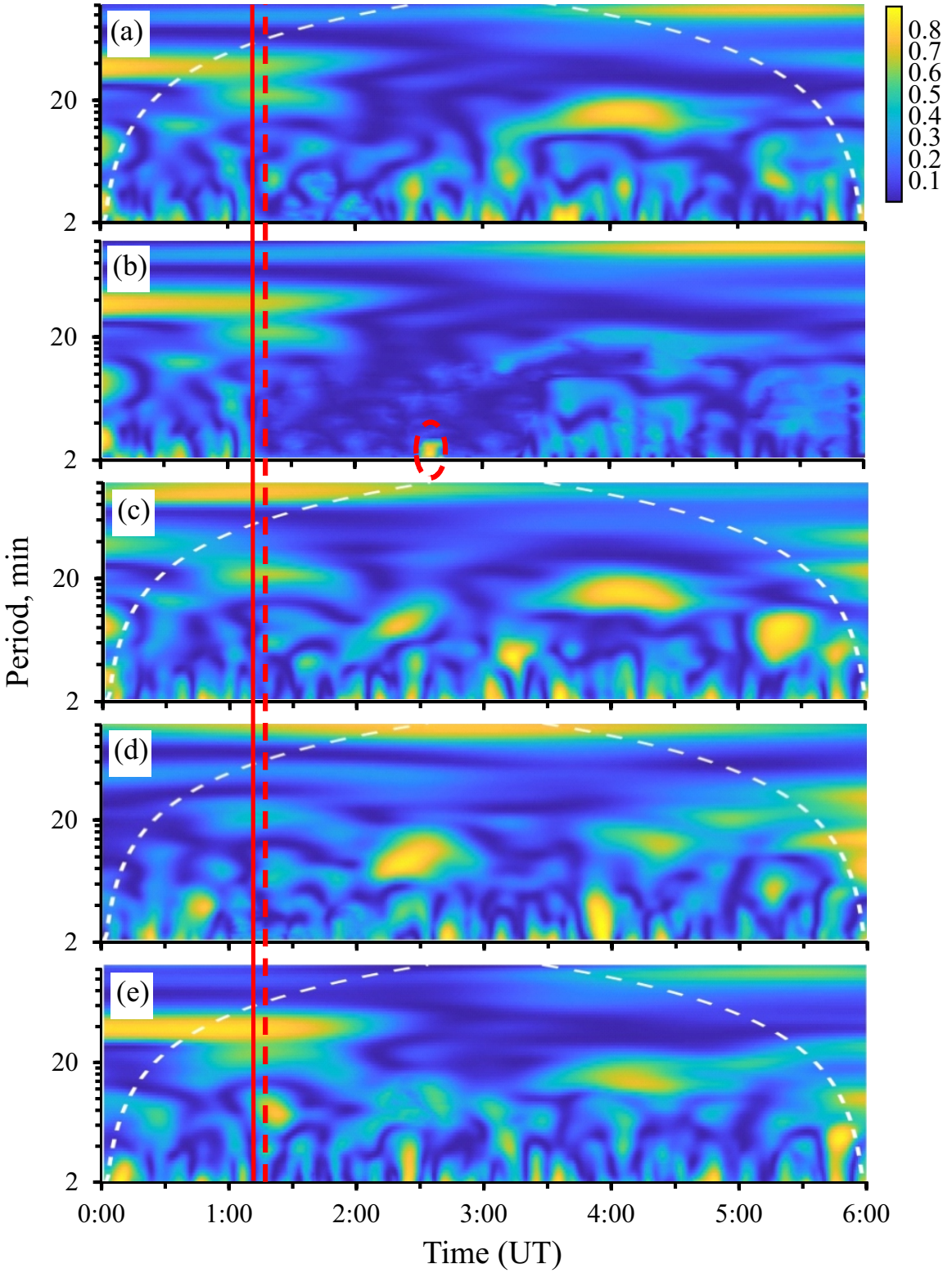

Figure 4. Cross-wavelet spectra between the B_z-component of the interplanetary magnetic field and northern (a), eastern (b) horizontal components, vertical component (c), total vector (d), horizontal component (e) of the magnetic field on the Earth's surface; red solid line is moment of main shock of the earthquake in Türkiye and Syria; red dashed line is moment of aftershock of the earthquake in Türkiye and Syria.

Türkiye and Syria and its strongest aftershock, we will take into account the eastern horizontal component of the magnetic field.

6. Results of the analysis of geomagnetic variations after the main shock

Considering that the registration of geomagnetic variations after the main shock showed a similar pattern for three stations: Grocka, Panagjurishte, and Surlari, we will discuss only case of the Surlari observatory, which is closest to the epicenter of the earthquake. The detail results of magnetic variation measurements after the earthquakes at the nearest and more distant stations are given in Table 1, in which we present start and end times, as well as the minimum and maximum values of the peak in scalogram (for example, marked with a black line on the scalogram in Figure 5).

It is important to note that the identification of anomalies accompanying the event can be difficult even in variations of the eastern horizontal component of the magnetic field. In order to search for and determine the frequency composition of a possible response of the geomagnetic field, a wavelet transform was carried out. The estimate of the local energy spectrum (scalogram) at the Surlari observatory is shown in Figure 5. The calculations were performed for 6 h from the beginning of the day on February 6, 2023. Analysis of the data presented in Figure 5 showed that a number of anomalies can be distinguished in the behavior of the eastern horizontal component of the magnetic field. The first disturbance with a period of 4–6 min appears in the scalogram 13 min after the main shock of the earthquake. The second signals with a period of 2–4 min can be identified in the scalogram approximately 11 min later than the first one. The third signal with a period of 11–20 min, arising 1 h 20 min after the main shock of the earthquake, stands out well in the scalogram. The presence of another increase (at about 2:40 UT) in the power spectrum is clearly associated with a solar source, which can be confirmed by the coincidence of the period of the high-coherence scalogram between the considered eastern component of the magnetic field on the Earth's surface and the B_z-component of the interplanetary magnetic field (Figure 4b). The increase in coherence corresponding to this anomaly is marked with a red oval in Figure 4b. Notice, that while the range of periods of this signal corresponds to the so-called acoustic resonance, which is sometimes associated with an earthquake (see, for example, (Matsumura et al., 2009)), but the distance from the epicenter of the event (approximately 1200 km) does not allow us to consider the earthquake as the cause of the signal.

Thus, in the eastern horizontal component of the Earth's magnetic field, near the epicenter of the earthquake in Türkiye and Syria (at the Surlari observatory) there are three anomalies: one with a period of 4–7 min occurring 12–15 min after the main shock of the earthquake, the other – 11 min later than the first anomaly with a period of 2–4 min, the third – with a period of 11–20 min, that occur 1 h 20 min – 1 h 40 min after the main shock. Note, that comparison with other days (before or after the day of the event) did not show any patterns of comparable intensity. Below, the reason for the abnormal signals will be discussed for all three stations in terms of propagating seismic Rayleigh waves and internal gravity waves generated by the earthquake.

7. Results of the analysis of geomagnetic variations after the strongest aftershock of the earthquake

In order to search for a geomagnetic response to the strongest aftershock with a magnitude 7.5, observations of geomagnetic variations at four observatories (Grotska, Panagyurishte, Surlari, and İznik observatories) were analyzed.

Table 1. Parameters of geomagnetic disturbances after main shock of the earthquake in Türkiye and Syria.

Observatory	Time (UT)		Period	
	Start	End	Maximum	Minimum
Surlari	1:29	1:38	3.83	5.42
	1:40	1:48	2.63	3.73
	2:36	2:40	2.29	2.84
	2:44	2:49	3.24	4
	2:30	3:35	11.31	19.82
Panagjurishte	1:29	1:39	4	6.49
	1:40	1:50	2.63	4.28
	2:36	2:40	2	2.64
	2:46	2:50	3.82	4.39
	2:32	3:23	11.12	18.52
Grocka	1:31	1:45	3.82	6.86
	1:42	1:51	2	3.24
	2:36	2:42	2	3.73
	2:50	4:19	10.72	18.27

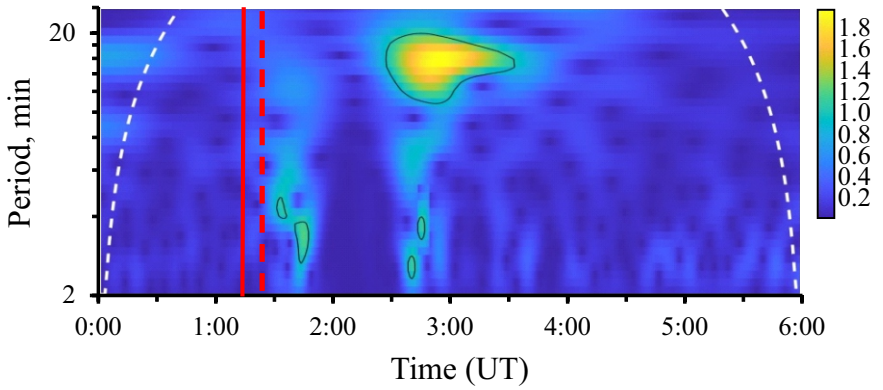

Figure 5. Scalogram of variations of the eastern horizontal component of the geomagnetic field on the Earth's surface according to the data of the Surlari observatory; red solid line is moment of the main shock of the earthquake in Türkiye and Syria; red dashed line is moment of the aftershock of the earthquake in Türkiye and Syria.

The estimation of the local energy spectrum (scalogram) at the nearest observatory to the epicenter – İznik observatory – is shown in Figure 6. Analysis of the data presented in Figure 6 showed that four anomalies can be distinguished in the behavior of the eastern horizontal component of the magnetic field. The first signal with a period of 2.3–4.5 min manifests itself in the scalogram 9 min after the aftershock. Approximately 45–50 min after the aftershock the second and third signals occur with a period of 3–4 min and of 28–50 min, respectively. And finally, the fourth anomaly with a period of 2.5–3.5 min occurs at 12:11 UT.

At more remote observatories (Grotska, Panagyurishte, and Surlari observatories) two perturbations appear in the scalograms (Table 2). The first signal occurs ~12–14 min after the strongest aftershock and has a period of 4–7 min. The duration of this disturbance is 10–30 min. The second long-period signal (the oscillation period lies in the range of 11–24 min) at the Surlari and Panagyurishte observatories occurs approximately 1 h and 20 min after the strongest aftershock. At the Grotska observatory, there is a delay in the occurrence of a long-period geomagnetic anomaly of 20–25 min compared to the geomagnetic variations recorded at the Panagyurishte and Surlari observatories. A long-period disturbance is longer than a short-period one. The duration of this disturbance is ~70–110 min, and the longest signal duration was observed at the Grotska observatory, the duration at the Panagyurishte and Surlari observatories is approximately the same.

8. Discussion of the results and conclusion

Let us consider the reasons for the signals observed by the ground-based magnetometers at the Grocka, Panagjurishte, Surlari, and İznik observatories.

In general, we await different kinds of ionospheric responses (disturbances of the ionospheric current can produce then ground based magnetic variations) associated with both the main shock and strongest aftershock and caused by different mechanisms. An earthquake epicenter is known to be a source of both seismic Rayleigh waves and atmospheric acoustic-gravity waves. The fastest is seismic Rayleigh waves (with velocity ~3–4 km/s), propagating in the solid Earth. Rayleigh waves serves as a source of atmospheric acoustic waves propagating upward and causing ionospheric disturbances. The internal gravity waves (IGWs) propagating from the epicenter take a longer time to reach the same region of the ionosphere, since the vertical and horizontal velocities of these waves (~40 m/s and ~150–300 m/s, respectively) are smaller than the speed of sound.

As follows from the previous consideration, the magnetometer at the Surlari observatory (see Figure 5), located at a distance of about 1200 km from the epicenter, registered the first signal with a period of 4–6 min just 12 min after the earthquake, the second – with a period of 2–3 min and 11 min later than the first one, and the third one with a period of 11–20 minutes 80 min after the main shock. In this case, the first and second disturbances are caused by the arrival of seismic Rayleigh waves at the Surlari observatory from the main shock and aftershock (with a magnitude of 6.7), respectively. Since this seismic wave propagates at a speed greater than the speed of sound, it generates an acoustic wave, which propagates into the ionosphere and leads to disturbances in the lower ionosphere via collisions of neutrals with ions. The third disturbance owes its appearance to the arrival of IGW propagating at velocities in the range of 200–300 m/s. This wave (with a period of about 20 min) enters the thermosphere at a distance of approximately 400 km from the epicenter. Its further propagation is possible in a thermospheric waveguide (see, for example, (Snively and Pasko, 2008)) associated with a rather narrow perturbation spectrum.

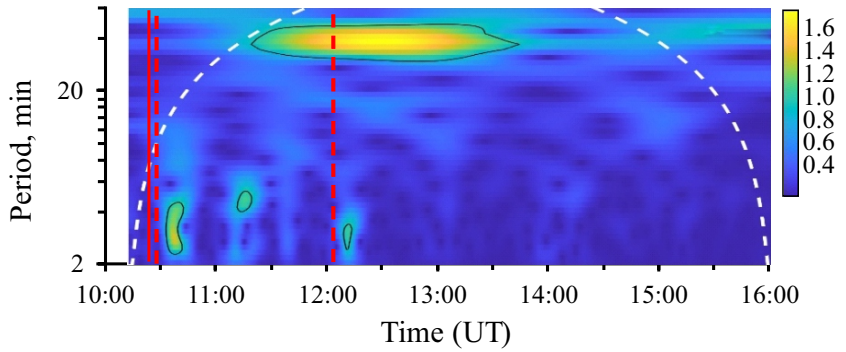

Figure 6. Scalogram of variations of the eastern horizontal component of the background geomagnetic field at İznik observatory; red solid line is a moment of strongest aftershock of the earthquake in Türkiye and Syria; red dashed lines are two more moments of aftershocks with magnitude 6.0.

Since the distance of the Panagjurishte station from the epicenter is approximately the same as for the Surlari, a similar pattern of magnetic disturbances can be expected. This is confirmed by the data presented in Table 1. On the other hand, the Grocka station is located several hundred km further from the epicenter than Panagjurishte and Surlari. Therefore, it can be expected that the propagation time to it of both the Rayleigh wave (with a velocity of about 3 km/s) and the internal gravity wave captured in the thermospheric waveguide will increase. This is exactly what was observed according to Table 1.

Now let us discuss magnetic signals observed after the strongest aftershock. For the İznik station closest to the epicenter of the strongest aftershock, it is necessary to take into account a shorter distance (700 km) for the propagation of the Rayleigh waves and the acoustic-gravity waves from the epicenters of the events. Therefore, we may await a more interesting spectrum of recorded signals. Indeed, the first signal is associated with the arrival of Rayleigh waves, propagating at a speed of 3 km/s and caused by the strongest aftershock followed by an earthquake with a magnitude of 6 (2 min later and slightly closer to the station İznik). The fourth signal is interpreted in the same way, taking the second event with a magnitude of 6 as a source. The second and third signals were recorded at the station at approximately the same time, but have significantly different spectral compositions. Both of these signals could be generated directly at the epicenter, and the short-period (acoustic) signal above the epicenter enters the thermosphere waveguide (Snively and Pasko, 2008), in which it propagates to the observation point, causing corresponding geomagnetic variations. A long-period signal, in accordance with the formula for internal gravity waves, must have an approximate period $T = T_g L/h$ above the observation point where T_g is the Brunt-Väisälä period, L, h is the distance from the source and the height of signal generation. Taking L = 700 km, h = 100 km, we find $T \approx 39$ min for signals at the İznik station, which is consistent with the experiment (see Figure 6 and Table 2).

Table 2. Parameters of geomagnetic disturbances after strongest aftershock of the earthquake in Türkiye and Syria.

Observatory	Time (UT)		Period	
	Start	End	Minimum	Maximum
Iznik	10:33	10:41	2.29	4.59
	11:11	11:20	4	5.28
	11:14	13:43	28.25	48.5
	12:11	12:17	2.46	3.48
Surlari	10:36	10:47	3.82	6.18
	11:39	12:49	10.84	24.18
Panagjurishte	10:37	11:02	4.35	5.84
	11:43	12:47	12.18	24.1
Grocka	10:39	11:05	4.32	6.86
	12:03	13:54	10.69	24.2

Let us now consider the results of recording geomagnetic variations after the strongest aftershock at the remote magnetic stations Surlari (distance 1175 km from the epicenter), Panagjurishte (1211 km), and Grocka (1553 km). The time of appearance of clear signals after the event is given in Table 2. Two types of signals were recorded at each station. The first signal at all stations corresponds to the arrival after the event of a Rayleigh wave propagating at a speed of 3 km/s. The second disturbance owes its appearance to the arrival of an atmospheric internal gravity wave propagating at speeds in the range of 200–300 m/s. This wave (with a period of about 15–20 min) enters the thermosphere at a distance of approximately 300–400 km from the epicenter. Its further propagation is possible in a thermospheric waveguide (see, for example, [Snively and Pasko, 2008]).

Thus, the general conclusion that follows from this work is the following: the ionospheric response to a sufficiently strong earthquake and its aftershocks in Türkiye and Syria, recorded at distances of 700–1600 km from the epicenter, is quite well interpreted in terms of propagation of secondary acoustic waves generated by seismic Rayleigh wave and atmospheric acoustic-gravity waves generated in the earthquake epicenter.

The studies were carried out within the framework of the state task of the IDG RAS (No. 1220329000185-5 "Manifestation of processes of natural and technogenic origin in geophysical fields") and within the framework of the state task of the IPE RAS. The authors are extremely grateful to Dr. Cengiz Çelik for providing magnetic recording data at the İznik Magnetic Observatory.

References

Adhikari B, Khatiwada R, Chapagain NP (2017). Analysis of geomagnetic storms using wavelet transforms. Journal of Nepal Physical Society 4 (1): 119–124. https://doi.org/10.3126/jnphyssoc.v4i1.17346

Chernogor LF (2019). Geomagnetic disturbances accompanying the Great Japanese earthquake of March 11 2011. Geomagnetism and Aeronomy 59 (1): 62–75. https://doi.org/10.1134/S0016793219010043

Daubechies I (1992). Ten lectures on wavelets. Philadelphia: SIAM.

Dautermann T, Calais E, Mattioli GS (2009). Global Positioning System detection and energy estimation of the ionospheric wave caused by the 13 July 2003 explosion of the Soufriere Hills Volcano Montserrat. Journal of Geophysical Research: Solid Earth 114 (B2): https://doi.org/10.1029/2008JB005722

Falayi EO, Adewole AT, Adelaja AD, Ogundile OO, Roy Layinde TO (2020). Study of nonlinear time series and wavelet power spectrum analysis using solar wind parameters and geomagnetic indices. NRIAG Journal of Astronomy and Geophysics 9 (1): 226–237. https://doi.org/10.1080/20909977.2020.1728866

Foufoula Georgiou E, Kumar P (1995). Wavelets in geophysics. New York: Academic Press.

Grinsted A, Moor JC, Jevrejeva S (2004). Application of the cross wavelet transform and wavelet coherence to geophysical timeseries. Nonlinear Processes in Geophysics 11 (5/6): 561–566. https://doi.org/10.5194/npg-11-561-2004

Grossmann A, Morlet J (1984). Decomposition of Hardy functions into square integrable wavelets of constant shape. SIAM Journal on Mathematical Analysis 15 (4): 723–736. https://doi.org/10.1137/0515056

Hao YQ, Xiao Z, Zhang DH (2013). Teleseismic magnetic effects (TMDs) of 2011 Tohoku earthquake. Journal of Geophysical Research: Space Physics 118 (6): 3914–3923. https://doi.org/10.1002/jgra.50326

Jackel BJ, McKiernan B, Singer J (2012). Geostationary magnetic field response to solar wind pressure variations: Time delay and local time variation. Journal of Geophysical Research: Space Physics 117 (A5): https://doi.org/10.1029/2011JA017210

Kelley MC (1989). The Earth's ionosphere: Plasma physics and electrodynamics. San Diego, California: Academic Press Inc.

Kunitsyn VE, Nesterov IA, Shalimov SL (2011). Japan mega-thrust earthquake on March 11 2011: GPS-TEC evidence for ionospheric disturbances. Journal of Experimental and Theoretical Physics Letters (JETP Letters) 94 (8): 616–620. https://doi.org/10.1134/S0021364011200082

Maraun D, Kurths J (2004). Cross wavelet analysis: significance testing and pitfalls. Nonlinear Processes in Geophysics 11 (4): 505–514. https://doi.org/10.5194/npg-11-505-2004

Maruyama T, Tsugawa T, Kato H, Ishii M, Nishioka M (2012). Rayleigh wave signature in ionograms induced by strong earthquakes. Journal of Geophysical Research: Space Physics 117 (A8): https://doi.org/10.1029/2012JA017952

Matsumura M, Iyemori T, Tanaka Y, Han D, Nose M et al. (2009). Acoustic resonance between ground and thermosphere. Data Science Journal 8 (9): 68–77. https://doi.org/10.2481/dsj.8.S68

Meyer Y (1993). Wavelets: Algorithms and applications. Philadelphia: Society for Industrial and Applied Mathematics.

Percival DB, Walden AT (2000). Wavelet methods for time series analysis. Cambridge: Cambridge University Press.

Riabova S (2018). Application of wavelet analysis to the analysis of geomagnetic field variations. Journal of Physics Conference Series 1141. https://doi.org/10.1088/1742-6596/1141/1/012146

Riabova SA (2022). Study of the multifractality of geomagnetic variations at the Belsk Observatory. Doklady Earth Sciences 507 (2): 299–303. https://doi.org/10.1134/S1028334X22700489

Riabova SA, Shalimov SL (2022). Geomagnetic variations observed on the Earth's surface and associated with strong earthquakes. Izvestiya Physics of the Solid Earth 58 (4): 469–483. https://doi.org/10.1134/S1069351322040085

Snively JB, Pasko VP (2008). Excitation of ducted gravity waves in the lower thermosphere by tropospheric sources. Journal of Geophysical Research: Atmospheres 113 (A6). https://doi.org/10.1029/2007JA012693

Spivak AA, Riabova SA (2019). Geomagnetic variations during strong earthquakes. Izvestiya Physics of the Solid Earth 55 (6): 811–820. https://doi.org/10.1134/S1069351319060077

Torrence C, Compo GP (1998). A practical guide to wavelet analysis. Bulletin of the American Meteorological Society 79: 605–618. https://doi.org/10.1175/1520-0477(1998)079<0061:APGTWA>2.0.CO;2

van Brummelen GR (2013). Heavenly mathematics: The forgotten art of spherical trigonometry. New Jersey: Princeton University Press.

Weimer DR, King JH (2008). Improved calculations of interplanetary magnetic field phase front angles and propagation time delays. Journal of Geophysical Research: Atmospheres 113 (A1). https://doi.org/10.1029/2007JA012452.

Zhao Y, Luo Y (2021). Wavelet analysis on temperature and precipitation changes in Dabie Mountain of West Anhui. Journal of Physics: Conference Series 1732 (1). https://doi.org/10.1088/1742-6596/1732/1/012105